

# TCAD analysis on the role of various layers in the improved internal gain of the avalanche photodiode

M. RIZWAN KHAN, M. FAHAD BHOPAL, M. ISHFAQ, J. A. ABBASI, A. S. BHATTI\*

*Centre for Micro and Nano Devices, Department of Physics, COMSATS Institute of Information Technology, Islamabad 44000, Pakistan*

State of the art industry standard Technology Computer Aided Design (TCAD) simulation tool was employed to optimize the silicon avalanche photodiode consisting of separate absorption, charge and multiplication layers (SACM-APD). The mobility, impact ionization and generation-recombination physics models were employed in various regions to maximize the performance of the device. The effect of widths of various regions like absorption, charge, and multiplication along with different doping profiles were simulated. It was demonstrated that a compromise was necessary between the widths of different regions to maximize the gain. To calculate the temperature dependence of IV curve, APD was simulated in the temperature range from  $-40^{\circ}\text{C}$  to  $60^{\circ}\text{C}$ . The breakdown thermal coefficient was  $0.034\%/^{\circ}\text{C}$ . The gain of the device showed more dependence on the electric field generated in the multiplication layer and a maximum gain of 96 with the electric field of  $4.1 \times 10^5 \text{V/cm}$  in the multiplication region was achieved. At that point, the peak optical responsivity of  $0.729 \text{ A/W}$  was also determined for the device. The present work has successfully demonstrated that there is still a room to fabricate high quality APD by precisely controlling the thicknesses and doping profiles of various layers.

(Received December 3, 2015; accepted August 3, 2016)

*Keywords:* SACM-APD, TCAD, Gain

## 1. Introduction

Photodiodes are widely used for the detection of visible and infrared radiation in a number of instruments and applications, e.g., photodiodes are an essential part in medical appliances for imaging and sensing, etc. [1]. Typically, photodiode has an absorption layer where optical signal is absorbed in the form of varied intensity and wavelength of incident photon. Each photon impinging on the absorption layer of the detector generates an electron-hole pair [2]. In many laser based systems like laser range finder, optical communication, etc., the incoming radiation intensity is quite weak and the detector with internal gain is needed. Avalanche photodiodes (APD) so far are the only detectors that have built in internal gain [3]. In APD, the generated charge carriers on exposure to radiations are multiplied. The two processes i.e., generation and multiplication of charges take place in different regions of the device. The photo-generated current is amplified by applying a high reverse bias voltage to the *pn* – junction, which induces the avalanche multiplication [4]. Avalanche breakdown occurs, when carriers generated by the incident radiation in absorption region of the device and are pushed into a region of high electric field, where carriers gain energy and collide with neutral atoms to release further charge carriers, a process known as impact ionization [5]. In the multiplication region, multiple impact ionizations can take place. The distance traveled by the carrier to attain sufficient energy that can produce impact ionizations is known as the dead

space [6], which is critical for the thickness of the multiplication layer and amplification of the detected signal. The continuous ionization process does not take place if the thickness of the multiplication layer is reduced to a few dead spaces [7,8]. The collision process for impact ionization repeats itself a number of times in an avalanche fashion eventually amplifying the signal, which makes the width of the multiplication region an important parameter to perform amplification for the detection of a weak signal.

Various kinds of APD structures have been modeled for the improved optical responsivity, low dark current, low signal to noise ratio, and high gain, etc. [9]. However, there still exists room for the optimum designed APD and its simulation for a specific application, e.g., determination of exact nature of the doping profile, geometrical dimensions of the device, etc., [10]. For example, experimental results and theoretical models have shown that small thickness of the multiplication layer resulted in the reduction of noise generated during impact ionization. Improved gain and the gain-band widths have been achieved by keeping the region thin [11,12]. Similarly, modifying the concentration of impurity levels in the absorption and multiplication regions resulted in the reduced dark current, and increased internal gain. This meant that for an optimized APD, a compromise between the various layer thicknesses and doping profiles in various regions has to be made. Electron hole pairs generation in the absorption layer due to thermal energy and other noise sources also contribute in the avalanche

breakdown process, and results in a small signal to noise ratio, etc. This very strongly implies the importance of simulation work to analyze and optimize the device parameters prior to its fabrication.

Industry standard Technology Computer Aided Design TCAD tool by Synopses was used to virtually fabricate and simulate the SACM-APD structure. Transport equations and physics models were employed, which governed the physical phenomena occurring in the device. The TCAD tool determines the transport of carriers from one point to another within the device by solving the Poisson and continuity equations in various layers [13]. The drift diffusion model was employed to determine current densities in different regions of the device, particularly in the multiplication region under various conditions. The electron mobility was determined as a function of temperature and carrier densities in various regions. In the multiplication region, avalanche generation model used for impact ionization was employed at high electric field. The generation recombination model was employed in absorption region, which was responsible for the generation of electron hole pairs by absorbing photon, thermal generation, etc. [13].

In this paper, SACM-APD studied systematically using TCAD by varying the thicknesses of absorption, charge and multiplication regions. The effect of thickness variation of any one of the region, and by keeping other region thicknesses fixed was studied on the electrical properties of the device. Current voltage (I-V) characteristics were analyzed for punch through voltage, breakdown voltage and the internal gain of the device, etc. On the basis of the analysis, an optimized structure of the device was predicted. Dark current, photocurrent, responsivity and the internal gain were measured for the proposed optimized APD structure. Some of the optimized characteristics were compared with the existing operating device.

## 2. Device structure

TCAD employs the fundamental physical phenomena that ultimately determine the response, performance and the production yield of useful devices. It, thus, acts as a bridge between the design and the fabrication. The design of the APD and modifications in it presented in the present work, have been done by virtually fabricating the device in the Sentaurus Structure Editor (SDE), a module for the fabrication of devices in the TCAD. The optimization of the device parameters and simulation was done with the Sentaurus Device (SD), Tecplot, etc., various modules of the TCAD [13].

The schematic cross-section of the device giving thicknesses of various regions with their doping profiles is shown in Fig. 1. The description of the device from bottom to top layers is also given in Table 1. The characteristics of the designed device was studied by employing specific physics models in specific regions of the device and introduced in the following section.

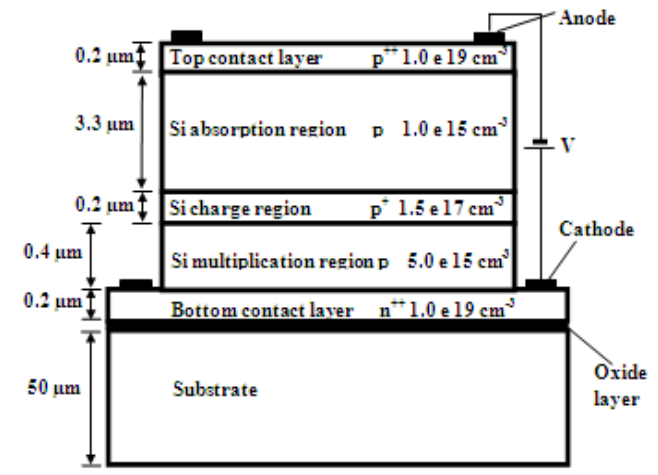


Fig. 1. Schematic cross section of SACM avalanche photodiode. The complete description of various layers is given in Table I.

## 3. Physics models

For the determination of optimally designed APD different physics models were employed that governed the device behavior like transport of charge carriers, generation and recombination, impact ionization, temperature dependent phenomenon like mobility, etc., in various layers. TCAD employs the Poisson and continuity equations for determination of transport of charge carriers in different regions of the device [13]. Electrostatic potential in the device is determined by the immobile ionized dopants, traps and charge carriers by solving the transport equations. The doping dependent properties, e.g., electric field profile, mobility, current densities, etc., were determined by the respective physics models. In the present device, the multiplication region doping was kept very low to enhance the mobility and reduce the scattering centers. Charge carriers gain kinetic energy under the influence of electric field and collide with neutral atoms to further release charge carriers by impact ionization, which was repeated across the full length of the multiplication region. In this region, avalanche generation model was employed to study the process of impact ionization [13].

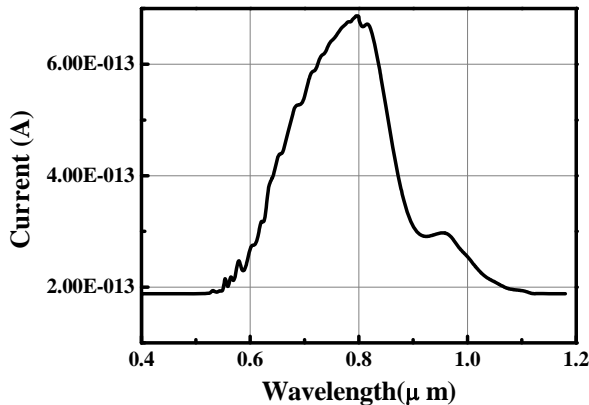
## 4. Results and discussion

The virtually designed device was characterized for its electrical and optical response in a systematic way. The effect of varying thicknesses of the absorption, charge and multiplication layers on the current – voltage (I-V) characteristics was studied at 300 K. The key parameters like layer thicknesses, doping profile, etc., were optimized to maximize the gain of the device. In the process of optimization, the thickness of one layer was varied while keeping thicknesses of other layers fixed. This allowed the study of the role of each layer independently and its effect of other layers. In the following, results are presented and discussed in detail.

#### 4.1 Optical characteristics

Fig. 2 (a) shows the optical response of the SACM-APD with dimensions given in Table 1 obtained at room temperature (300K) and at a reverse bias voltage of  $V_R = 65V$ . The curve showed a peak current value at a wavelength of  $0.8 \mu m$ , typical for Si. The value of peak responsivity of the device measured was  $0.729 AW^{-1}$ , obtained by dividing the total peak current by the incident optical power. In the responsivity curve, a kink was also observed at around  $1.0 \mu m$ , which was due to the doping level in silicon.

The magnitude of the dark and photocurrents were determined by sweeping the reverse voltage from zero to the breakdown voltage, where an abrupt increase in the current was observed just beyond  $65 V$  in the present designed device as shown in Fig. 2 (b). Both the photocurrent (red) and the dark current (black) increased in the region from  $12V$  to  $65V$ . At  $12V$ , a sharp step in the current was observed, which is known as the punch through voltage, at which the space charge region extended in to the absorption region.

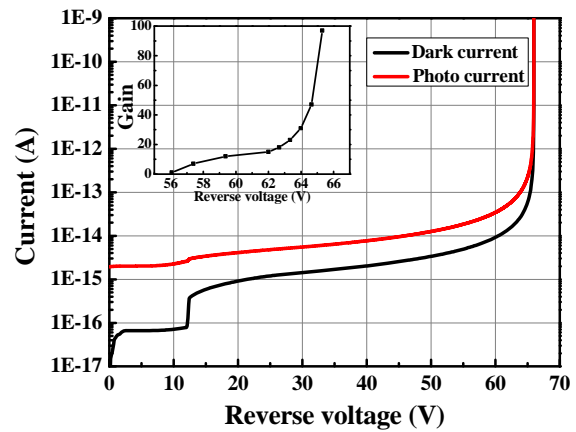


(a)

Table 1. SACM avalanche photodiode layers with thickness and doping profile.

Layer	Thickness	Doping ( $cm^{-3}$ )
Substrate	$50\mu m$	n-type $1 \times 10^{15}$
Cathode	$0.2 \mu m$	n-type $1 \times 10^{19}$
Multiplication	$0.4 \mu m$	p-type $5 \times 10^{15}$
Charge	$0.2 \mu m$	p-type $1.5 \times 10^{17}$
Absorption	$3.3 \mu m$	p-type $1 \times 10^{15}$
Contact	$0.2 \mu m$	p-type $1 \times 10^{19}$

Beyond the punch through voltage, the difference between the two curves reduced gradually as the reverse voltage was increased and almost merged at the breakdown voltage. The reduction of the difference in the magnitudes was due to the domination of noise multiplication over the photo-generated charge multiplication at a high electric field of about  $4.1 \times 10^5 V/cm$ .



(b)

Fig. 2. (a) Optical response curve of the SACM-APD obtained at room temperature. (b) Dark and photocurrents of the proposed APD at room temperature. The inset shows the gain of the device at different reverse bias voltages.

The multiplicative gain of the device was measured from the ratio of the difference of the both, i.e., the dark and photocurrents to the dark current of the device and is shown in the inset of Fig. 2 (b) as a function of the reverse bias voltage. The plot showed that with the increase of the reverse voltage, the gain of the device also increased. This trend was linear up to  $62V$  where the value of the gain reached to 12. But beyond  $62 V$ , the gain of the device increased abruptly and at  $65V$ , a gain of 96 was observed. In order to understand the behavior of the gain as a function of reverse bias, the profile of the electric field in various regions was determined at various reverse bias voltages and is shown in Fig. 3.

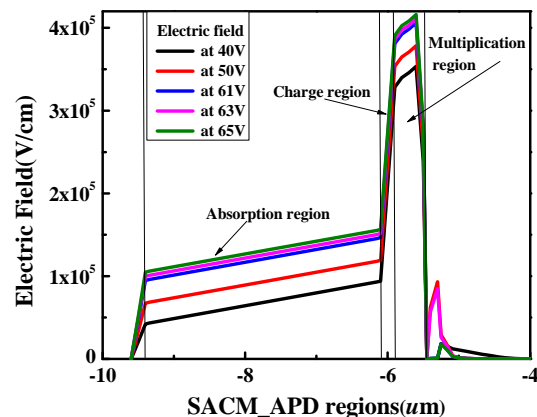


Fig. 3. Electric field profile in different regions of the APD obtained for different applied voltages.

The profile of the electric field in various regions revealed that the field strength was the highest in the multiplication region. On the other hand, the electric field gradient was the maximum in the charge region and a slight positive electric field gradient was observed in the absorption region, which was good enough to provide drift force to the photogenerated electrons to move towards the multiplication region. For higher values of applied voltages the electric field increased but the slope of the electric field profile remained unchanged and was found to be  $1.25 \times 10^{10}$  V/cm<sup>2</sup> in the charge region. The measured value of the maximum electric field in the multiplication region was  $4.1 \times 10^5$  V/cm, which was strong enough to increase the drift velocity of carriers and enhance to initiate the process of impact ionization needed for the avalanche breakdown phenomena. In addition, some random spikes were observed in the contact region, which were found to be SiO<sub>2</sub> layer dependent and arose due to defect-trapped charges of the oxide layer. In the absence of SiO<sub>2</sub> layers, these spikes disappeared.

#### 4.2 Electrical characteristics

The performance of any optoelectronic device depends on the magnitude of the dark current, which reflects its thermal behavior and stability. The magnitude of the dark current was determined by varying the thicknesses of various layers. The effect of varied thickness of the absorption region on the current-voltage (I-V) characteristics of the proposed device taken at 300K is shown in Fig. 4. The width of absorption region was varied from 1.7  $\mu\text{m}$  to 3.7  $\mu\text{m}$ , while widths of charge and multiplication regions were kept fixed at 0.2  $\mu\text{m}$  and 0.4  $\mu\text{m}$ , respectively.

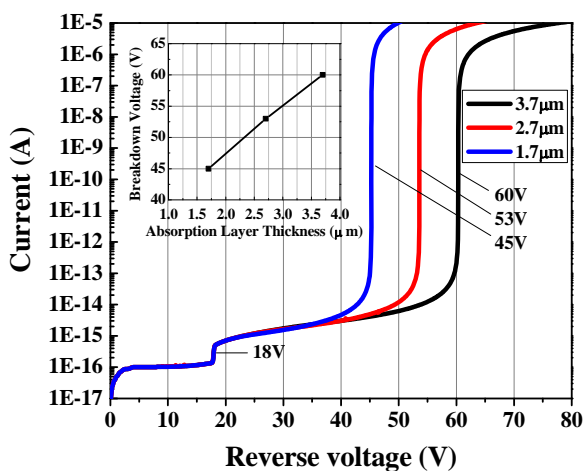


Fig. 4. I-V characteristics of the proposed device for different thickness of absorption region. The inset shows the variation of avalanche voltage as a function of the thickness of the absorption region.

The general trend for all absorption region widths was identical except that the breakdown voltage increased with the increase in the width. The punch through voltage for all widths was observed at 18 V and showed that it was independent of the absorption width. The observed change in the current up to 36 V was similar for the values of absorption thicknesses. However, a clear difference in the multiplicative gain was observed, where the breakdown voltage increased linearly with the increase in the absorption region as shown in the inset of Fig. 4. It implied that a better control of the gain characteristics could be achieved by changing the thickness of absorption layer.

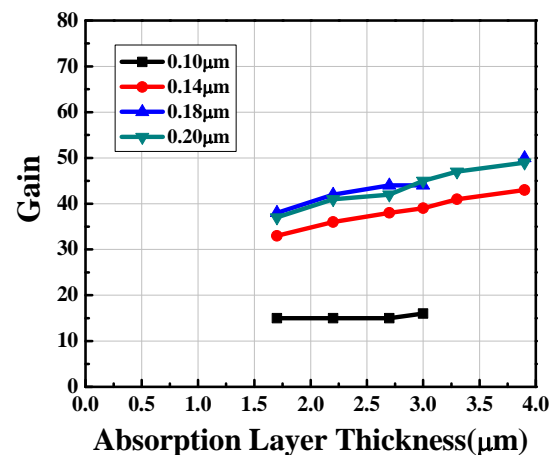


Fig. 5. Variation in the gain of the device obtained for different thicknesses of absorption layer.

However, increase in the width of the absorption region beyond a certain width possess a disadvantage that it affects the speed of the device, as the photo-generated electron-hole pairs take longer time to reach the respective electrodes. On the contrary, reduced width of the absorption region would also reduce the quantum efficiency of the device. This meant that it was necessary to reach a compromise for the appropriate thickness of the absorption region with a reasonable breakdown voltage and with high quantum efficiency [11]. Fig. 5 shows the effect of width of the charge region on the gain of the device for various absorption layer thicknesses. In these calculations, multiplication region thickness was fixed at 0.4  $\mu\text{m}$  and the charge region thicknesses were varied from 0.10  $\mu\text{m}$  to 0.20  $\mu\text{m}$ . The photocurrent and the dark current were measured at the 98% of the breakdown voltage to determine the gain of the device.

Fig. 5 shows the gain of the device as a function of absorption layer, where different symbols represent various thicknesses of the charge layer. The gain showed very little dependence on the absorption layer thickness, however, the gain increased when the charge layer thickness was increased. For the difference of 0.04  $\mu\text{m}$  from 0.10 to 0.14  $\mu\text{m}$  of charge layer thickness, the gain increased sharply, while for the same difference, a small

change in the gain was observed when charge region thickness was changed from  $0.14\ \mu\text{m}$  to  $0.18\ \mu\text{m}$ . The gain of the device was observed to change with the charge region thickness and this led to study the device by varying the charge layer thickness.

The charge region of the device is always sandwiched between the absorption and the multiplication regions with a comparatively high  $p$ -doping. The magnitude of the photocurrent and the change in the breakdown voltage was determined by varying the width of the charge region with a fixed  $p$ -type doping concentration of  $1.5 \times 10^{17}\ \text{cm}^{-3}$ . The results of current and breakdown voltage thus obtained are shown in the Fig. 6 and its inset, respectively. It can be seen that the punch through voltage of the device increased from  $5.5\ \text{V}$  to  $22.4\ \text{V}$ , while the breakdown voltage dropped from  $112.0\ \text{V}$  to  $70\ \text{V}$  and both trends are plotted in the inset of Fig. 6. It was found that the punch through voltage increased at a rate of  $52.0\ \text{V}/\mu\text{m}$  and the breakdown voltage dropped at a rate of  $59.3\ \text{V}/\mu\text{m}$ . This clearly demonstrated the effect of varied thickness of charge layer as it had a positive impact on the punch through voltage and an adverse effect on the avalanche breakdown voltage. The difference between the punch through voltage and the breakdown voltage for any curve is also an important parameter for the device. I-V characteristics displayed in Fig. 6 showed that the increase in the thickness of the charge region resulted in the decrease of the voltage gap between the punch through voltage and the breakdown voltage. Thus, it was concluded that the electric field required for the photogenerated electrons to achieve sufficient energy for the impact ionization could be attained at low voltages by increasing the thickness of the charge region.

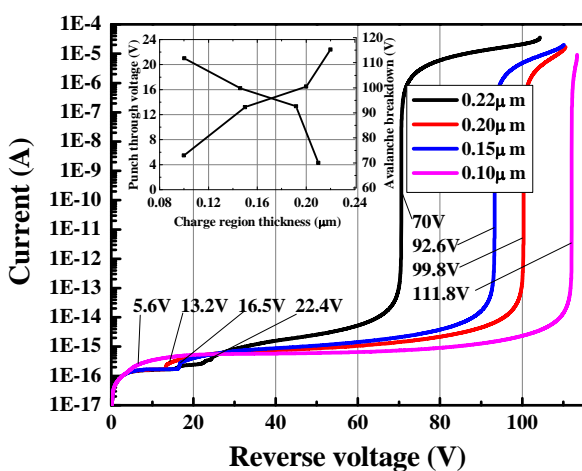


Fig. 6. I-V characteristics for different thickness of charge region. The inset shows the variation of the avalanche breakdown and punch through voltages as a function of the thickness of the charge region against.

In the charge region, electric field of the device increased sharply due to high doping and attained a maximum value of about  $4.1 \times 10^5\ \text{V}/\text{cm}$ . The high electric field played an important role in the multiplication of photo-generated carriers. The change of thickness of the charge region altered the maximum electric field, which affected the gain of the device. Fig. 7 (a, b) represent the multiplicative gain as a function of the charge region thicknesses for fixed thicknesses of the multiplication layer of  $0.8\ \mu\text{m}$  (Fig. 7 (a)) and  $0.4\ \mu\text{m}$  (Fig. 7 (b)), respectively. Different symbols corresponded to different absorption layer thicknesses as mentioned in the insets of the two figures.

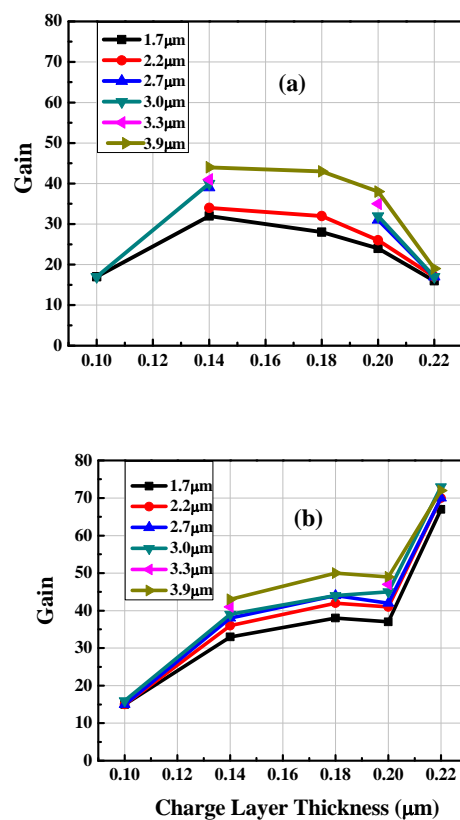


Fig. 7. (a) Variation in the gain of the device for different thicknesses of the charge layer for the fixed thickness of the multiplication layer at  $0.8\ \mu\text{m}$ . (b) Gain of the device for different thickness of charge layer keeping multiplication layer constant of  $0.4\ \mu\text{m}$ .

Fig. 7 (a) shows that the gain was stable and constant in the region where the charge layer thickness varied from  $0.14\ \mu\text{m}$  to  $0.20\ \mu\text{m}$  and then it dropped drastically below 20 when the charge layer thickness increased beyond  $0.20\ \mu\text{m}$ . This was the case when multiplication layer thickness was kept fixed at  $0.8\ \mu\text{m}$ . The drop in the gain was further investigated for different value of multiplication layer thickness i.e.,  $0.4\ \mu\text{m}$ . However, as shown in Fig. 7 (b), when the width of the multiplication region was reduced to  $0.4\ \mu\text{m}$ , initially the gain was stable in the region between  $0.14\ \mu\text{m}$  to  $0.20\ \mu\text{m}$  of the charge layer thickness and the

behavior was more or less similar to what was observed in Fig. 7(a), but it showed an abrupt increase in the gain beyond  $0.2 \mu\text{m}$ , due to domination of the photo-generated multiplication processes over the excess noise generation. From these results, it was concluded that thickness of the charge region up to  $0.20 \mu\text{m}$  was sufficient to produce the maximum possible electric field in the region, however, the gain of the device was highly dependent on the multiplication region. In the next phase, the gain was determined for different thicknesses of the multiplication region. In the multiplication region, the electric field remained almost constant to the maximum value attained at the interface of the charge and multiplication regions. Thus, an appropriate thickness of the multiplication region was required for the maximum gain without generating excess carrier noise.

Fig. 8 shows the characteristic I-V curves measured for different widths of the multiplication region, namely from  $0.1 \mu\text{m}$  to  $1.0 \mu\text{m}$ . The general trend for all widths of the multiplication regions was identical except that the breakdown voltage decreased drastically from  $89 \text{ V}$  to  $49.6 \text{ V}$  and punch through voltage increased from  $4.2 \text{ V}$  to  $30 \text{ V}$  with the increase in the thickness of the multiplication region.

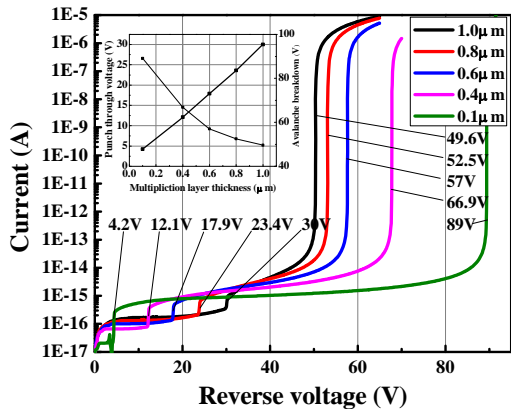


Fig. 8. The plot of I-V curves obtained for different thicknesses of the multiplication region. The inset shows the variation of the punch through and avalanche voltage as a function of thickness of the multiplication region.

The variations in the punch through and the breakdown voltages as a function of the multiplication layer thickness are plotted in the inset of Fig. 8. The punch through voltage increased linearly with a slope of  $28.6 \text{ V}/\mu\text{m}$  of the multiplication region width, while the breakdown voltage decreased exponentially having an exponent of  $-0.4$  with the increase in the thickness of multiplication region. This was further investigated to determine the effect of multiplication layer on the gain of the device for varied thicknesses of the absorption layer while keeping the charge layer thickness fixed at  $0.18 \mu\text{m}$  (Fig. 9 (a)) and  $0.20 \mu\text{m}$  (Fig. 9 (b)).

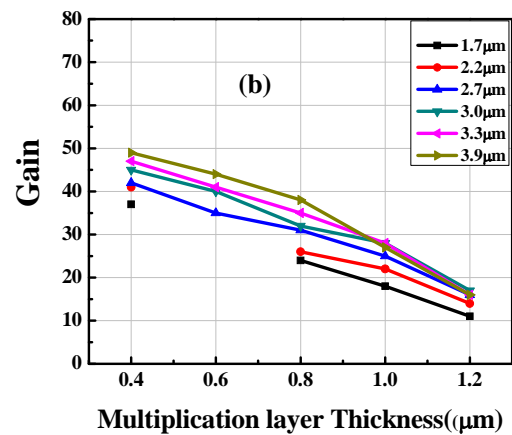
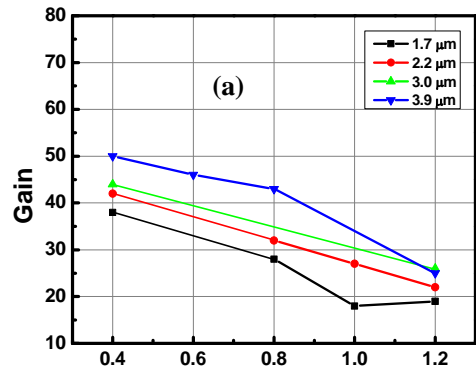


Fig. 9. (a) Gain of the device for different thicknesses of the multiplication layer obtained by keeping charge layer thickness fixed at  $0.18 \mu\text{m}$ . (b) Gain of the device for different thicknesses of the multiplication layer obtained by keeping charge layer thickness fixed at  $0.20 \mu\text{m}$ .

The gain of the device was greatly affected by the increased multiplication region as excess noise was generated in this region. In order to reduce the source of noise, the multiplication layer thickness was reduced to a  $0.1 \mu\text{m}$ , which is still larger than the dead space. It was concluded that multiplication thickness should not be more than a few multiples of dead space, where the excess noise becomes insignificant. A much thicker multiplication region would lead to generation of excess noise degrading the performance of the device.

The device was also characterized for the thermal effects by taking the I-V curves at various operating temperatures in the range from  $242 \text{ K}$  to  $323 \text{ K}$  and the response is shown in Fig. 10. It was observed that the current of the device increased with the increase in temperature. The punch-through voltage of the device remained independent of the operating temperature while the avalanche breakdown voltage increased with the increase in temperature. The random noise in the curve observed for  $243 \text{ K}$  just before the punch through voltage was due to current fluctuations in the device at low temperatures. At low temperature, the ionization of donor states was incomplete, which could lead to fluctuation in current. However, at elevated temperatures, ionization

process was complete and hence no fluctuation was observed.

The breakdown voltage thermal coefficient was determined to be 3.4 mV/K by using the following equation [14]:

$$\delta = \left( \frac{\Delta V_{bd}}{V_{bd}} \right) / \Delta T$$

The measured value showed that the change in the avalanche breakdown voltage per degree change in temperature was 0.034 %/°C, better than observed experimentally and it also showed that silicon has a very low temperature dependent breakdown shift as reported earlier [14].

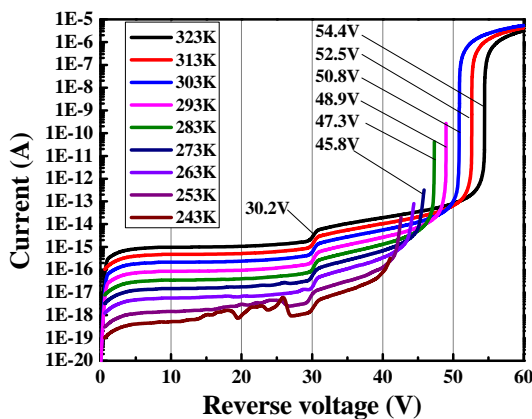


Fig. 10. The plot of I-V curves obtained at various operating temperatures of the device as mentioned in the figure.

## 5. Conclusion

In the present work, state of the art Technology Computer Aided Design (TCAD) tool was used to simulate silicon avalanche photodiode with separate absorption, charge and multiplication layers. The mobility, impact ionization and generation-recombination physics models were employed in various regions of the device to study the behavior of the proposed device. For optimum performance of the device, widths of various layers like absorption, charge and multiplication along with their varied doping profiles were simulated. It was observed that for the best performance, a compromise between the thicknesses of various layers had to be made. I-V characteristics of the device were simulated to optimize the layer thicknesses. Device was also characterized for optical behavior at different operating voltages and different incident optical powers. Gain of 96, breakdown thermal coefficient 0.034%/°C and responsivity 0.729 A/W was measured for the optimized device. These results confirmed that there is still quite a room to improve the performance of the practical device by varying the thicknesses of various layers.

## Acknowledgment

The research was funded by the Higher Education Commission of Pakistan through its Development grant "Designing and fabrication of micro and nano devices." One of the author MRK is thankful to IICS for PhD scholarship.

## References

- [1] W. William Moses, Nucl Instrum Methods Phys Res A, **610**(1), 11 (2009).
- [2] F. Träger, Handbook of Lasers and Optics, Springer, 2007.
- [3] J. C. Campbell, Journal of Lightwave Technology, **25**(1), 109 (2007).
- [4] Mohd Azlishah Othman, Siti Nabilah Taib, Mohd Nor Husain, Zul Atfyi Fauzan Mohammed Napiiah, ARPN Journal of Engineering and Applied Sciences, **9**(1), (2014).
- [5] V. Chandramouli, C. M. Maziar, J. C. Campbell, IEEE Transactions on Electron Devices, **41**(5), 648 (1994).
- [6] P. J. Hambleton, B. K. Ng, S. A. Plimmer, J. P. R. David, G. J. Rees, IEEE Transactions on Electron Devices, **50**(2), 347 (2003).
- [7] R. J. McIntyre, IEEE Transactions on Electron Devices, **46**(8), 1623 (1999).
- [8] Sungmin Hwang, Jongin Shim, Kyungyul Yoo, Journal of the Korean Physical Society, **49**(1), 253 (2006).
- [9] A. Rochas, A. R. Pauchard, P. -A. Besse, D. Pantic, Z. Prijic, R. S. Popovic, IEEE Transactions on Electron Devices, **49**(3), 387 (2002).
- [10] G.-F. Dalla Betta, S. Ronchin, A. Zoboli, N. Zorzi, Microelectronics Journal, **39**, 1485 (2008).
- [11] P. Yuan, K. A. Anselm, C. Hu, H. Nie, C. Lenox, A. L. Holmes, B. G. Streetman, J. C. Campbell, R. J. McIntyre, IEEE Transactions on Electron Devices, **46**(8), 1632 (1999).
- [12] P. Yuan, C. C. Hansing, K. A. Anselm, C. V. Lenox, H. Nie, A. L. Holmes, B. G. Streetman, J. C. Campbell, IEEE Journal of Quantum Electronics, **36**(2), 198 (2000).
- [13] Synopsys TCAD, webpage <http://www.synopsys.com>.
- [14] Y. Kang, M. Zadka, S. Litski, G. Sarid, M. Morse, M. J. Paniccia, Y.-H. Kuo, J. Bowers, A. Beling, H. D. Liu, D. C. McIntosh, J. Campbell, A. Pauchard, Optics express, **16**(13), 9365 (2008).

\*Corresponding author: asbhhatti@comsats.edu.pk